Reconstruction de la variation de la concentration en ion CO_3^{2-} des eaux profondes du Pacifique Est tropical au cours des transitions MIS 12 et 11 et MIS 16 et 15

Introduction

Les carottes de sédiment marin ont permis de mettre en évidence la forte variabilité du climat au cours des derniers 800 ka et au-delà. Ainsi, au cours du Pléistocène supérieur, on observe de grands cycles, qualifiés de glaciaires-interglaciaires de par la présence de calottes plus ou moins étendues aux hautes latitudes, avec une cyclicité de l'ordre de 100 000 ans (Hays et al., 1976). Cette variabilité se caractérise par de fortes variations du volume des glaces et de la température, et aussi par de fortes variations des concentrations en gaz à effet de serre dans l'atmosphère, comme l'ont montré les enregistrements des carottes de glace antarctiques (Petit et al., 1999 ; Jouzel et al., 2007 ; Luethi et al., 2008) (Figure 69). Ces grands cycles montrent une très forte corrélation entre volume des calottes de glace et concentration en CO_2 de l'atmosphère. Or l'atmosphère est un réservoir de carbone relativement restreint par rapport à l'océan, principal réservoir avec lequel elle peut échanger du carbone aux échelles de temps décennales à millénaires. Ainsi, on suppose que la majorité du carbone relargué dans l'atmosphère au cours des différentes déglaciations provient de l'océan, et notamment de l'océan profond.

De nombreuses études ont porté sur la reconstruction de la variation du contenu en carbone de l'océan profond au cours de ces grandes transitions du Pléistocène supérieur. Mais les proxies étaient le plus

souvent indirects et relativement peu quantitatifs. Ainsi, par exemple, plusieurs de ces études ont-elles porté sur les variations de saturation des eaux de fond (qui dépend de la concentration [CO_3^{2-}]) reconstruites à partir du seul pourcentage en $CaCO_3$ des sédiments (e.g. Farrell and Prell, 1989; Hodell et al., 2001). L'hypothèse à la base de cette approche, est que la teneur en $CaCO_3$ des carottes sédimentaires dépend essentiellement des processus de dissolution/préservation, et donc de l'état de saturation des eaux de fond. Or, la teneur en $CaCO_3$ des sédiments ne dépend pas que des changements de la dissolution elle dépend également de la productivité de particules calcaires en surface ainsi que de la dilution par les particules non-carbonatées (e.g. argiles, silice biogène). Quelques études plus récentes ont utilisé des proxies plus quantitatifs et plus directement associés à la saturation des eaux de fond comme le poids des tests de foraminifères, le rapport Mg/Ca des foraminifères benthiques, le rapport Zn/Ca ou encore l'isotopie du bore (e.g. Broecker and Clark, 2001 ; Elderfield et al., 2006 ; Marchitto et al., 2005 ; Hönisch et al., 2008, respectivement), chacun de ces proxies présentant leurs avantages et leurs inconvénients que nous détaillerons dans ce chapitre.

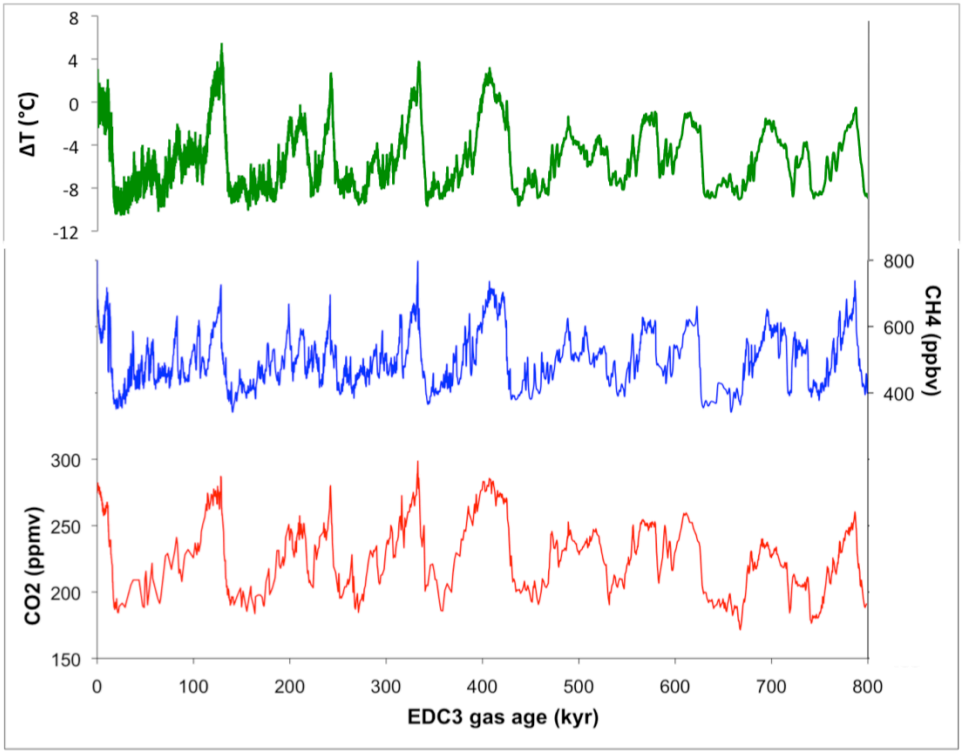

Figure 69 : Evolution des concentrations atmosphériques de méthane et de CO_2, ainsi que différences de température par rapport à la moyenne des derniers 1000 ans (calculées à partir du δD) au cours des derniers 800 ka, obtenues à EPICA Dome C. Données de CO_2 de Monnin et al. (2001), Petit et al. (1999), Siegenthaler et al. (2005), Luethi et al. (2008) ; données de CH_4 de Loulergue et al. (2008) ; données de température de Jouzel et al. (2007).

Le rapport B/Ca des foraminifères benthiques représente un proxy idéal pour reconstruire la variation du contenu en carbone des eaux profondes. En effet, ce proxy permet de reconstruire l'état de saturation en ion carbonate des eaux de fond (Yu et Elderfield, 2007) et donc d'en dériver directement la concentration

en ion carbonate (Yu et al., 2010 ; Raitsch et al., 2011). Or, par exemple, une émission intense de carbone de l'océan vers l'atmosphère va perturber les équilibres chimiques régissant la spéciation du carbone dans l'océan, et donc modifier notamment les concentrations de CO_3^{2-}. L'espèce *C. wuellerstorfi* (Figure 70) est idéale pour ce type de reconstruction, en raison de sa relative forte teneur en B/Ca (de 140 à 250 µmol/mol), de sa forte sensibilité au variations de saturation des eaux de fond comparativement aux espèces *Cibicides kullenbergi* ou *Uvigerina perégrina* (Yu et al., 2007) (Figure 71). De plus elle est epibenthique et son rapport B/Ca ne sera donc pas influencé par la concentration en ion carbonate des eaux interstitielles.

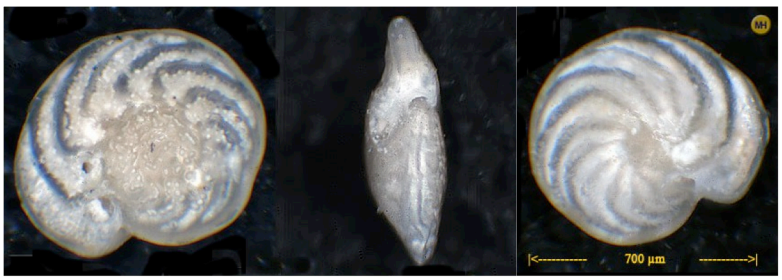

Figure 70 : Photos d'un test de foraminifère benthique de l'espèce *Cibicides wuellerstorfi*. Disponible à : http://www.foraminifera.eu/cibicides.php

Dans le cadre de cette thèse, nous nous sommes intéressés à reconstruire l'évolution de la concentration en ion carbonate dans l'océan pacifique profond au cours de deux déglaciations, les transitions entre les stades isotopiques marins MIS 12/11 et MIS 16/15. Entre 400 et 800 ka, les variations de la pCO_2 atmosphérique durant les déglaciations était de l'ordre de 80 ppm, tandis que pour les transitions plus récentes (0-400 ka) cette variation était de 100 ppm (Figure 69). Nous avons donc choisi d'étudier deux transitions qui sont chacune typique de ces deux périodes : transition MIS 16/15, associée à un changement de 80ppm de la pCO_2 atmosphérique, et la transition MIS 12/11, qui est la première du Pleistocène supérieur à montrer une variation pCO_2 de 100 ppm. L'objectif de cette étude est de mettre en évidence les variations de la concentration en ion carbonate au cours de ces deux transitions, ainsi que les différences entre les deux transitions qui seraient à même d'expliquer la différence de variation de pCO_2 observée.

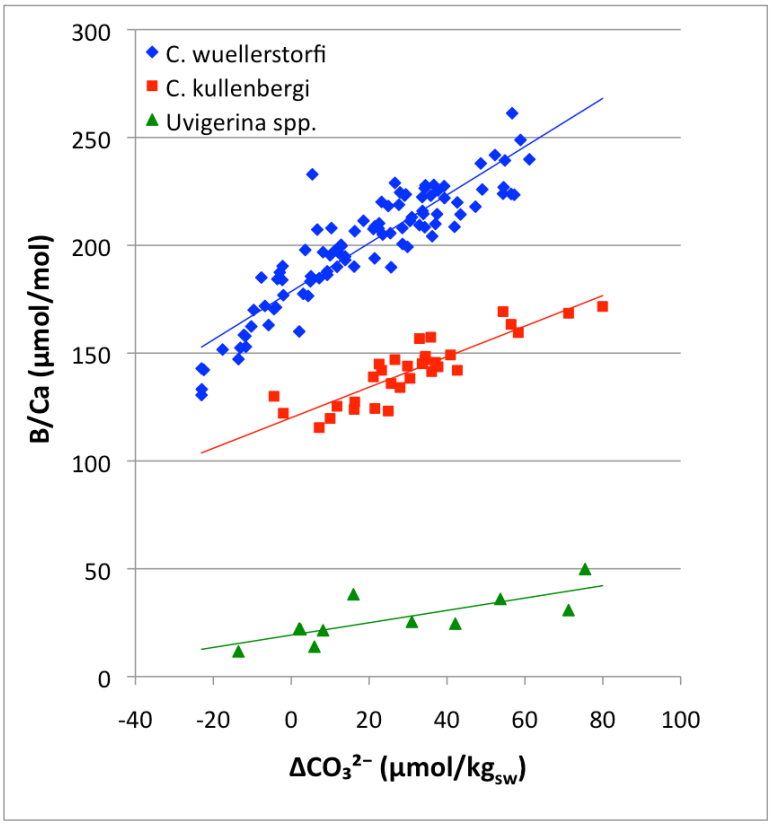

Figure 71 : Rapport B/Ca en fonction de la saturation en ion carbonate vis-à-vis de la calcite, ΔCO_3^{2-}, pour les deux espèces de foraminifères *C. wuellerstorfi*, *C. kullenbergi* et pour les espèces regroupées sous *Uvigerina spp*.. Les droites sont les régressions linéaires des données. Modifié d'après Yu et Elderfield (2007).

Pour mener à bien ce genre d'étude, les sédiments déposés dans l'océan Pacifique constituaient une cible privilégiée. En effet, l'Océan Pacifique profond n'est que peu impacté par les variations de circulation océanique au cours des déglaciations. Contrairement à l'Océan Atlantique, par exemple, où les changements glaciaires/interglaciaires s'accompagnent d'importantes variations dans l'importance relative et la composition de plusieurs masses d'eaux très contrastées (e.g. North Atlantic Deep Water, Antarctique Bottom Water), l'Océan Pacifique profond est plus représentatif des changements de composition chimique à grande échelle de l'océan mondial.

Ce chapitre est présenté en anglais, et rédigé sous forme de publication scientifique qui sera soumise très rapidement à une revue internationale

Deep Tropical Pacific carbonate preservation changes over glacial-interglacial transitions MIS 12/11 and MIS 16/15

1. Introduction

Analysis of air trapped in ice cores through the last 800,000 years showed the importance of greenhouse gases such as CO_2 for the regulation of climate on glacial/interglacial (G/IG) time scales (Lüthi et al., 2008). These data clearly showed that orbitally-driven insolation changes alone cannot explain G/IG changes and that the carbon cycle is a key element at a deglaciation timescale. The ocean is the largest reservoir that can rapidly exchange carbon with the atmosphere. It is believed to play a major role in G/IG climatic changes. The pelagic deep-sea carbonates can potentially buffer ocean pH changes through the dissolution or preservation of carbonates on the sea floor. This effect counteracts or amplifies the changes in the ocean carbon budget. Changes in ocean pH and dissolved carbonate speciation provide a mechanism to maintain a balance between inputs of dissolved carbonate species to the ocean and their removal through the burial of sediments (the so-called *carbonate compensation*). Several paleoceanographers have tried to evaluate the role of the ocean carbonates on carbon atmospheric composition for the G/IG transitions of the late Pleistocene (e.g. Sigman et al. 2010, 2000 for reviews). However, most of these studies are only qualitative, and we still need to better understand and to quantify the ocean carbon chemistry variations involved in the G/IG changes.

Several studies focused on the calcium carbonate content (%$CaCO_3$) of the deep-sea sediments to determine past changes in the dissolution at the seafloor, which is highly related to the carbonate saturation state of deep waters (i.e. Farrell and Prell, 1989; Hodell et al., 2001). However, this proxy is not an unambiguous proxy of dissolution/preservation since it also depends (1) on the surface productivity, as well as (2) on dilution by non-carbonate material, which may both vary during G/IG transitions. Other proxies have been developed to reconstruct the dissolution/preservation signal of deep-sea pelagic carbonates, such as: (i) the foraminifer fragmentation (Berger et al., 1979; Le and Shackleton, 1992), (ii) the relative amount of the coarse fraction (Berger et al., 1982; Peterson and Prell, 1985, Wu et al., 1990; Bassinot et al., 1994); (iii) the size-normalized, foraminifer shell weight (Lohmann, 1995; Broecker and Clark, 2001, 2002), (iv), and the foraminifer calcite crystallinity (Bonneau et al., 1980; Bassinot et al., 2004; Nouet and Bassinot, 2007). However, if all these proxies are indeed strongly affected by carbonate dissolution, they are also affected by other mechanisms that can potentially bias past dissolution/preservation reconstructions. For instance, (i) the initial planktonic foraminifer shell weights may depend on surface ocean [CO_3^{2-}] (Barker and Elderfield, 2002), (ii) foraminifer fragmentation may

depend upon the initial composition of assemblages, and (iii) the % coarse fraction may be affected by surface productivity, dilution by fine, non-carbonate material or the winnowing at the sea bottom.

The isotopic composition of boron ($\delta^{11}B$) included into the $CaCO_3$ produced by marine organisms has proved to be a reliable proxy of seawater pH and hence carbonate ion. It has been used with success with coral aragonite (Vengosh et al., 1991; Hemming and Hanson, 1992) and could be used for foraminifer calcite as well (Hönisch et al., 2008; Yu et al., 2010; Rae et al., 2011). However, the still relatively large amount of calcite required for $\delta^{11}B$ analyzes makes it difficult to apply this approach for the reconstruction of deep-water chemistry due to the scarcity of benthic foraminifers.

More recently, proxies based on trace element composition of foraminifer shells have been scrutinized for paleo- CO_3^{2-} reconstructions. It has been suggested, for instance, that the Mg/Ca of benthic foraminifers depends strongly upon bottom water ΔCO_3^{2-} (Elderfield et al., 2006; Yu and Elderfield, 2008). However, it is hard to deconvolve this effect from the temperature effect on Mg/Ca. Marchitto et al. (2005) used the Zn/Ca ratio of the benthic species *Cibicidoides wuellerstorfi* picked from deep-sea sediments to reconstruct the saturation state of bottom seawater at three Pacific sites. However, this proxy presents two disadvantages: (i) the potential Mn-Ca-carbonate overgrowths can contaminate the calcite with Zn, hence preventing the use of the Zn/ca proxy in case of high Mn/Ca, and (ii) the Zn/Ca relationship to bottom carbonate saturation is limited to the -20 to 20 µmol/kg range of ΔCO_3^{2-}, thus making it difficult or even impossible to apply this proxy for the reconstruction of shallow Pacific and/or Atlantic bottom water ΔCO_3^{2-}.

More recently, Yu and Elderfield (2007) have shown that the B/Ca of benthic foraminifers reflects the carbonate saturation state of deep water (ΔCO_3^{2-}). The precise measurement of B/Ca by ICP-MS requires only a small amount of calcite (150 to 200 µg). Despite the difficulties linked to boron analysis (Yu et al., 2005), B/Ca has proved to be a reliable tool to reconstruct bottom water saturation state, with no dependency on the surface fluxes and no contamination from secondary calcite overgrowth. The empirical relationship between carbonate saturation and B/Ca ratio of the benthic species *C. wuellerstorfi*, the most sensitive species to saturation changes and with the highest B/Ca ratio of the investigated species, can be expressed as (Yu and Elderfield, 2007):

$$B/Ca = 1.14\ \Delta CO_3^{2-} + 177.1 \qquad (1)$$

Furthermore *C. wuellerstorfi* is an epibenthic species and will therefore reflect the bottom water carbonate saturation without being influenced by the pore water chemistry. Since the seminal work of Yu and Elderfield (2007), the B/Ca of *C. wuellerstorfi* has been used in two recent studies to reconstruct past variations of the carbonate saturation state of deep-waters since the last glaciation (Yu et al., 2010; Raitsch et al., 2011) and it has also been used to reconstruct glacial-interglacial, bottom water ΔCO_3^{2-}

changes over the last 800 kyr, but with an average time-resolution of only about ~ 15 kyr (Rickaby et al., 2010).

Here, we present a high resolution *C. wuellerstorfi* B/Ca record from the equatorial Pacific core ODP 849 for the transitions between marine isotopic stages 12 and 11 (MIS 12/11) and between MIS 16/15. The G/IG transition MIS 12/11, also known as termination V, is interesting because, as shown by Antarctic ice records, it is the first of recent Pleistocene G/IG transitions to present a high-amplitude, G/IG pCO_2 variation of ~100 ppm, typical of the recent deglaciations (Lüthi et al., 2008; Figure 72). Moreover, this transition is considered by several paleoceanographers as an analogue to termination I (TI; the last deglaciation), which was recently analyzed by Yu et al. (2010) using the B/Ca proxy. We decided to compare the MIS 12/11 transition to the MIS 16/15 transition, which is more representative of the deglaciations occurring from 450 to 800 ka, and characterized by an atmospheric pCO_2 change with a lower amplitude (i.e. a ~80 ppm change across MIS16/15).

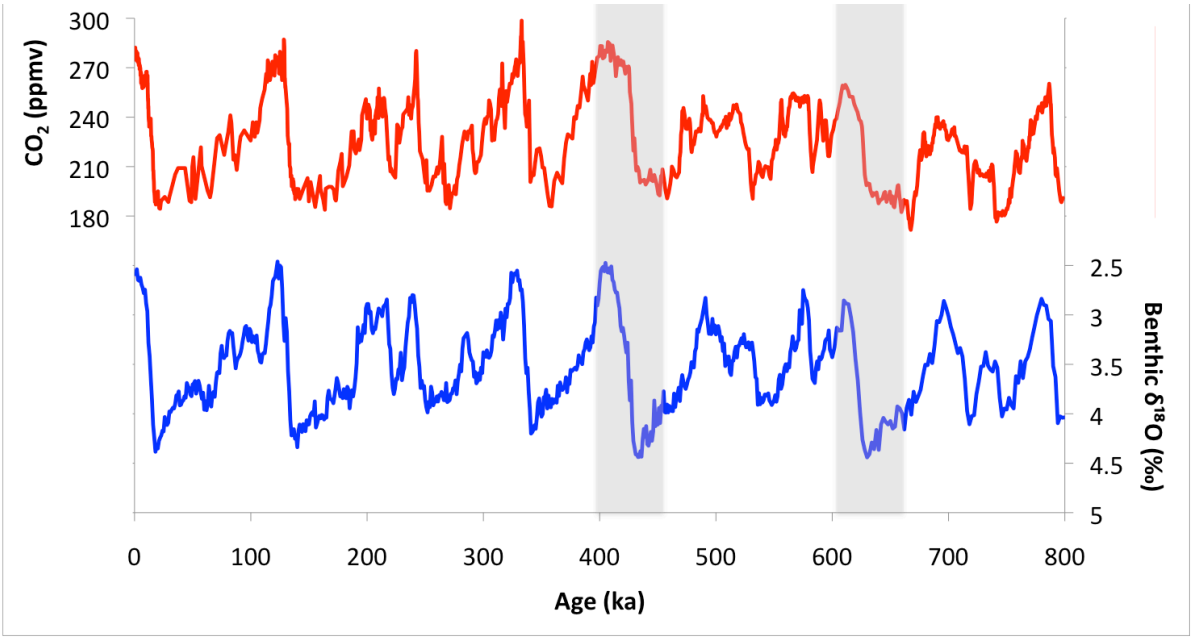

Figure 72 : Composite concentration of CO_2 for the upper Pleistocene record in Vostok and Epica Dome C ice cores (Lüthi et al., 2008) (upper curve, red) and bentic oxygen isotopic composition from the LR04 bentic stack (Lisiecki and Raymo, 2005) (lower curve, blue). Light, vertical gray bars are centered on the MIS 12/11 and MIS 16/15 transitions, respectively.

Following the strategy from Yu and coworkers (2010), we will compare our B/Ca record to the benthic foraminifer $\delta^{13}C$ record. In addition, we will also compare our B/Ca data to four carbonate proxies, namely: the percentage of calcium carbonate, the percentage of coarse fraction, shell fragmentation and foraminiferal shell weight. This comparison will make it possible to better understand to which extend the B/Ca signal is coherent with these well-known proxies, that have been used for many years to derive past history of deep-sea water saturation changes.

Our comprehensive dataset will make it possible: 1/to derive some new insights into differences and similarities provided by different proxies on changes in deep-water saturation; 2/ to quantify Pacific bottom ΔCO_3^{2-} changes and highlight similarities and differences of deep-sea carbonate chemistry evolution across two mid-Pleistocene G/IG transitions characterized by different amplitudes in atmospheric pCO_2 changes; 3/ to compare the deep-sea chemistry evolution at these transitions to that from the last deglaciation, recently studied by Yu et al (2010) using the same approach.

2. Material and methods

2.1. Oceanographic settings and presentation of ODP 849 site

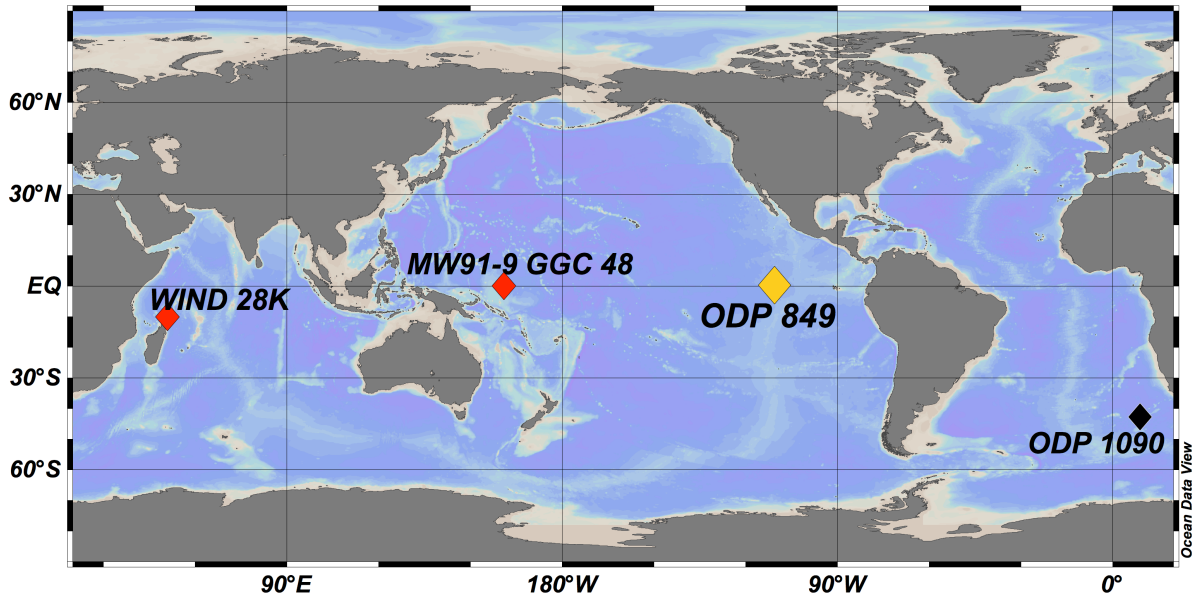

Figure 73 : Locations of cores discussed in this study

Core ODP 849 is situated in the eastern deep tropical Pacific, at a water depth of 3839m (Figure 73). This 343 m thick sedimentary section covers from 3ka to up to 11Ma and was built from successive, 10m-long hydraulic piston cores recovered at four holes, and spliced to obtain a continuous record. The splicing of the cores was made on-board using magnetic susceptibility, colorimetry and density (GRAPE: Gamma Ray Attenuation Porosity Evaluator) measurements (Leg 138, Initial Report Proceeding of the ODP, 1991). A biostratigraphic age model was developed during the cruise based on microfaunal changes. Mix et al. (1995) proposed another age model for the last 5Ma based on oxygen isotopic measurements of benthic

foraminifera and its tuning to orbital forcing functions. This age model shows a mean sedimentation rate of ~2.9 cm/kyr for the last 800kyr. The benthic isotope stratigraphy made it possible to identify the two transitions MIS 16/15 and MIS 12/11.

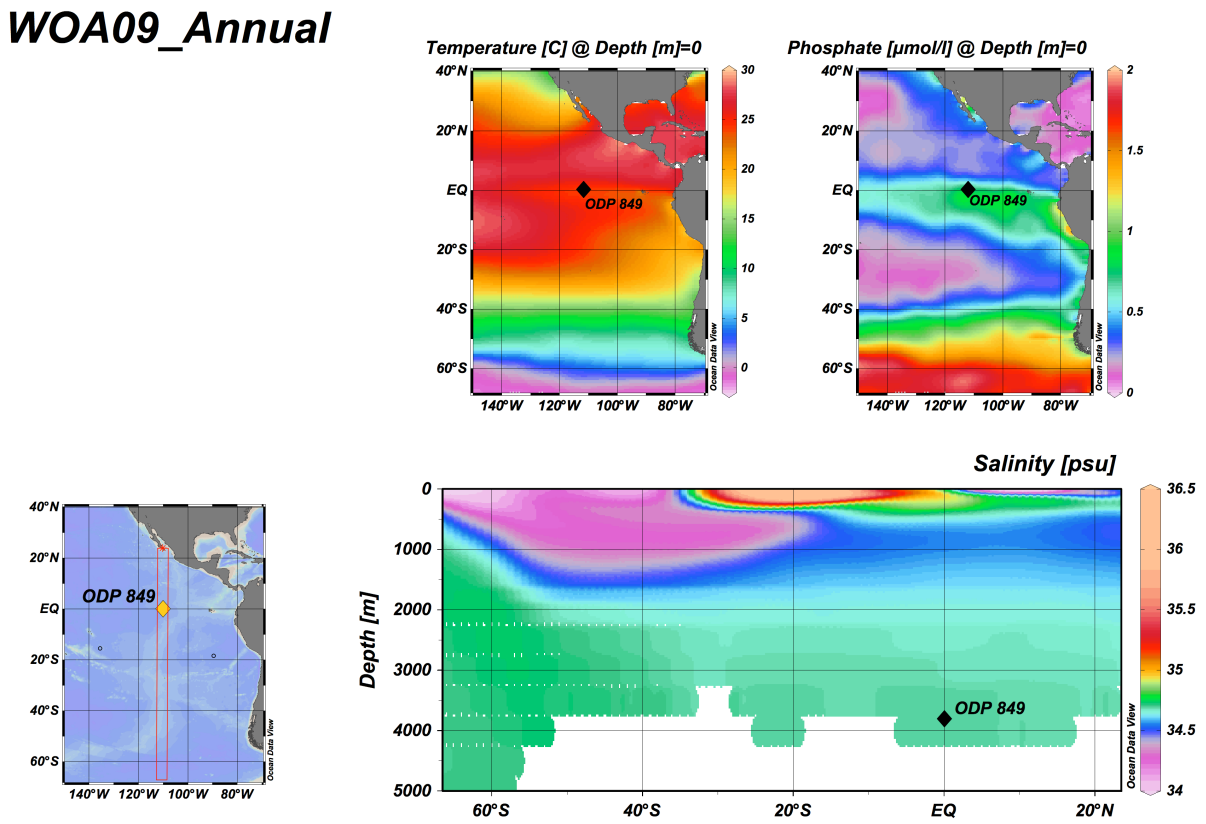

Figure 74 : Sea surface temperature (°C) and phosphate concentration (µmol/kg) in the area of Site ODP 849, and salinity (‰) along a North-South east Pacific transect. Red line indicates the section investigated, black diamonds indicate the depth and position of Site ODP 849. Data are form World Ocean Atlas 2009 (Boyer et al., 2009).

Site ODP 849 is bathed by the Antarctic bottom water, and is situated slightly south-west to the equatorial east Pacific upwelling (Figure 74). According to the GLODAP dataset (Key et al., 2004), the bottom water temperature is ~1.5°C, with a salinity of ~34.7. We combined alkalinity (2435 µmol/kg) and pre-industrial values of dissolved inorganic carbon (DIC, 2335 µmol/kg) to calculate bottom water carbonate ion concentration and the actual carbonate saturation state (ΔCO_3^{2-}) at this site. Results show a modern, bottom water [CO_3^{2-}] of ~80µmol/kg, which corresponds to a ΔCO_3^{2-} of -10µmol/kg, which is in good agreement with the relatively poor preservation of the pelagic carbonate material noticed on-board, as expected for a deep-sea Pacific core.

2.2. Oxygen and carbon isotope measurements

Oxygen isotopic and carbon isotopic ratios were obtained on 1 to 4 shells of the benthic species *Cibicidoides spp.* Shells were ultrasonically cleaned in a methanol bath to remove clays and other impurities. They were roasted under vacuum at 380°C during 45 min to eliminate organic matter. Samples were analyzed with an IsoPrime mass spectrometer. All results are expressed as $\delta^{18}O$ and $\delta^{13}C$ in ‰ versus V-PDB with respect to NBS 19 and NBS 18 standards. The analytical reproducibility as determined from replicate measurements of a carbonate standard is ±0.09‰ and ±0.1 ‰ (2σ), and the mean standard deviation of replicate analyses performed on several foraminifer samples is 0.11‰ and 0.13 ‰ (2σ) for oxygen and carbon isotopic compositions, respectively.

2.3. The B/Ca ratio of benthic foraminifer shells

Approximately 3 to 10 individuals (typically >150µg of calcium carbonate) of *C. wuellerstorfi* were handpicked from the >150 µm size-fraction, and weighed using a precision microbalance. The main difficulties at the ODP Site 849 are the relatively poor abundance of this benthic species, and the greater morphological similarity between *C. wuellerstorfi* and *C. kullenbergi* (*C. mundulus*) than in previously studied cores (Rae et al., 2011). Hence, we selected only the *sensu stricto* morphotypes of *C. wuellerstorfi*. Because of the paucity of this morphotype, we had to combine several, 1cm-thick adjacent samples over some intervals in order to get the necessary amount of material for B/Ca analyses. This is particularly the case for MIS 12/11, hence explaining the lower temporal resolution we achieved over this transition. The standard deviations on the depths retained after combining adjacent samples for B/Ca measurements represent 3.3 cm and 2.6 cm for MIS 12/11 and MIS 16/15, respectively.

The cleaning protocol of foraminifer shells for B/Ca analyses was derived from the Mg/Ca-cleaning method of Barker et al. (2003). The *C. wuellerstorfi* shells were gently crushed in order to open the chambers and allow any chamber fill to be removed during the following cleaning steps. After crushing, clays were removed by successive Milli-Q water and ethanol ultrasonic washes, and an oxidative step (H_2O_2, 100°C) was applied in order to remove organic matter. Finally, a leaching with a dilute nitric acid (0.001 M HNO_3), was performed to remove any contaminants that may have been adsorbed onto the shells. Prior to analysis, samples were dissolved in 250 µL of 0.1M HNO_3 acid.

An aliquot of each sample solution was diluted and measured using an inductively coupled plasma – atomic emission spectrometer (ICP-AES), to determine its calcium concentration. Based on this measurement, the calcium concentration of each sample was adjusted to 100 ppm by dilution, and the sample was run on a Xseries^{II} (Thermo Analytical) inductively coupled plasma – quadrupole mass spectrometer (ICP-QMS). Setting the Ca concentration of calibration solutions and samples to 100 ppm makes it possible to overcome matrix effects while determining trace elements (Bourdin et al., 2011; Harding et al., 2006) or more specifically B/Ca and Mg/Ca ratios (de Villiers et al., 2002; Yu et al., 2005). During the final run, the B/Ca were estimated using an intensity ratio calibration method (de Villiers et al., 2002).

In order to reduce the boron background level and the memory effect, a mini cyclonic quartz chamber with an inner tube and a Teflon nebulizer were used. Prior to analysis, we performed a cone-conditioning step following the procedure described by Yu et al. (2005). In addition to analyzing a reference calibration solution during the run, we also measured the B/Ca ratio of a coral powder reference material (JCp-1; Okai et al., 2002, 2004) every five samples and that of a giant clam powder material (JCt-1; Okai et al., 2004) every ten samples as previously described by Bourdin et al. (2011). These reference points showed that the drift along a typical analytical session (~6 hrs) was less than 5% for boron and 1% for magnesium. Moreover, a blank was analyzed before each sample to monitor the potential influence of the memory effect. The standard reproducibility, based on ~100 replicate measurements of the giant clam powder material JCt-1 (Okai et al., 2004), is 3.5% (2σ) for B/Ca measurements and 1.5% (2σ) for Mg/Ca measurements with mean values of 197 µmol/mol and 1.28 mmol/mol, respectively. The simultaneous measurement of the JCt-1 material (~5 times per day of analysis) makes it possible to scale the results of different days analysis to a JCt-1 value of 189.8 µmol/mol.

2.4. Sedimentological proxies of dissolution

2.4.1. Percentage of calcium carbonate

The relative weight percentage of $CaCO_3$ in 50 ODP 849 samples was estimated using a carbonate-bomb calcimeter. For this purpose, 100mg of dried bulk sediment was ground and reacted with HCl 6N acid in a 22.4 cm^3 reaction-chamber equipped with a manometer. The pressure generated by the CO_2 outgassing was measured to obtain the $CaCO_3$ concentration in the sediment with a precision of ± 2% (2σ). Pure calcite was measured every five samples to correct for potential drifts associated to changes in room temperature or ambient pressure. The use of the calcimeter gives a smoother record than the percentage of $CaCO_3$ obtained through GRAPE (Gamma Ray Attenuation Porosity Evaluator) measurements (Mayer, 1991; Leg 138, Initial Report Proceeding of the ODP, 1991)

2.4.2. Fragmentation of foraminiferal shells and percentage of coarse fraction

Bulk samples were dried (24h at 50°C), weighted and gently wet-sieved with a paintbrush on a 150µm mesh-sieve in order to retrieve foraminifer shells and avoid any mechanical fragmentation that could bias the sedimentological dissolution proxies. The percentage of the coarse fraction (>150µm) was calculated as the ratio between the dry mass of particles over 150 µm and the initial dry mass of the bulk sediment sample:

$$\text{Fraction} > 150\ \mu m\ (\%) = 100 * (M_{>150\mu m} / M_{\text{total sediment}}) \qquad (3)$$

As far as foraminifer fragmentation is concerned, a minimum of 300 particles was counted under a binocular for each sample in the >150 µm size-fraction in order to achieve a good statistical

representativeness. For some samples, up to 10 replicates were counted to evaluate the repeatability of this technique, leading to a mean uncertainty of ± 5% (2σ).
The percentage of foraminifer fragmentation is computed as follow:

Fragmentation (%) = 100 * (foraminifer fragments / (fragments + whole shells)) (3)

Such as proxy gives a "dissolution" index, for which high values indicate a high level of fragmentation and, therefore, a strong carbonate dissolution at the seafloor. In the present study, this proxy will be plotted with a reversed Y-axis, in order to mimic variations in the other proxies (which are carbonate "preservation" proxies).

2.4.3 Foraminifer shell weights

The post-deposition loss of carbonate through dissolution was shown to affect the size-normalized weigth of foraminifers shells (Lohmann et al., 1995). For ODP 849 samples, we used the planktic species *Neogloboquadrina dutertrei*, which is abundant all along the two studied transitions. For each sample, about ~25 individual shells were handpicked under a binocular in the narrow size fraction 355-400 µm. They were weighed using a precision balance to determine the mean weight of each individual. Multiple replicates performed on several samples provided a mean uncertainty of ± 5% (2σ) on the individual foraminifer weight estimation.

3. Results

3.1. Oxygen and carbon isotopes

In the MIS 12/11 transition, oxygen isotopic records of the benthic species *Cibicides spp.* and *Uvigerina spp.* and on the planktonic species *Neogloboquadrina dutertrei* have shown an anomalous interval between 1349 to 1369 cm, characterized by high-amplitude, erratic changes. This interval did not show up on the lower resolution isotopic stratigraphy established by Mix et al. (1995). This depth interval corresponds to the limit between two sections from adjacent holes spliced together to construct the composite sedimentary column. Looking more carefully at the high-resolution GRAPE and color reflectance data used on board ODP Leg 138 we could establish a better composite record by suppressing the disturbed part on the top of the deeper section. Hence, we decided to suppress the depth interval 1349-1369 cm (composite depth), and to correct the composite depth by subtracting 20 cm downcore.

For the transition 16/15, we examined also precisely the transition between two sections. High-resolution B/Ca results show a ~6 cm shift between the B/Ca variations of the two sections, where they overlap each other (from 1873 to 1916 cm, 15 points per section). This shift is also seen using on-board high resolution measurements of density and colorimetry, hence, we decided to correct the composite depth scale by subtracting these 6 cm from the section situated below 1873 cm to obtain a better overlap between the two sections.

Because we measured B/Ca on the epibenthic species *C. wuellerstorfi*, we present here the *Cibicidoides spp*. $\delta^{18}O$ record. The oxygen and carbon isotopic composition of this benthic species are displayed versus depth on figure 75. In both transitions, $\delta^{18}O$ reaches nearly identical values at peak glacials, with values of 4.2‰ and 4.3‰ for transitions MIS 16 and MIS 12, respectively. At the onset of the deglaciations, $\delta^{18}O$ decreases rapidly and reaches minimum values of 2.8‰ and 2.3‰ at peak interglacial MIS15 and MIS11, respectively. Thus, the amplitude of $\delta^{18}O$ deglaciation signal is only 1.4‰ across the MIS16/15 transition, whereas it reaches 2‰ across MIS12/11.

During the glacials, $\delta^{13}C$ shows little variations. During MIS 16, $\delta^{13}C$ shows a minimum of -0.5 ‰ at 1940 cm; before increasing slowly to -0.3‰ and reach a second minimum of -0.5‰ at ~1850 cm. This second minimum marks the beginning of the deglaciation increase in $\delta^{13}C$, which reaches its highest value (0.2‰) during MIS 15, at 1815 cm. During MIS 12, $\delta^{13}C$ also presents two minimum values of -0.6 and -0.5 ‰ at 1410 and 1320 cm, respectively. This second minimum also marks the beginning of deglaciation increase in $\delta^{13}C$, reaching 0.5 ‰ at 1260 cm.

For both G/IG transitions, we used the period of heaviest/minimum $\delta^{18}O$ values as stratigraphic references for the full glacial and interglacial, respectively. Theses periods are indicated by light grey dashed rectangles on figure 75. Considering these stratigraphic references, the amplitude of the G/IG $\delta^{13}C$ change appears to be 0.5‰ for MIS16/15 and 0.8‰ for MIS12/11. During the two deglaciations, the $\delta^{18}O$ change leads the $\delta^{13}C$ change, with relatively stables $\delta^{13}C$ values during the first part of the deglaciation before $\delta^{13}C$ increase in its second part.

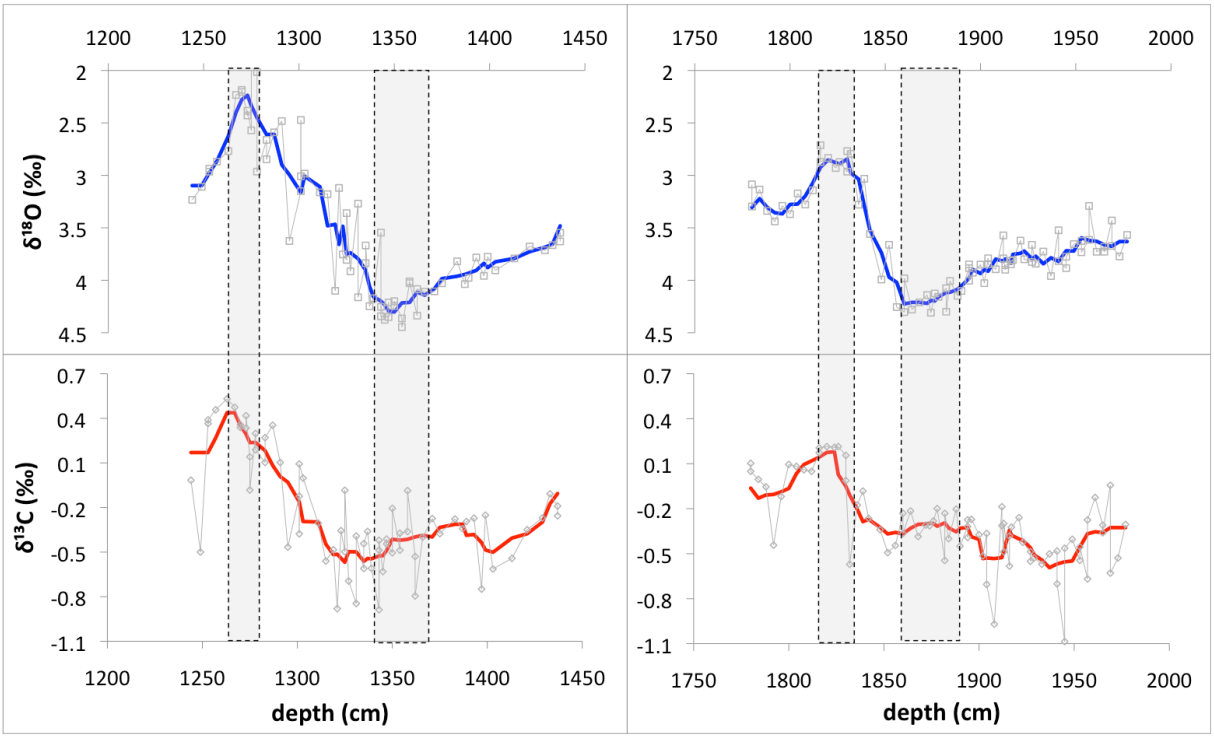

Figure 75 : Oxygen isotopic composition $\delta^{18}O$ and carbon isotopic composition $\delta^{13}C$ of the benthic species *Cibicidoides spp.* over the transitions MIS 16/15 (right panels) and MIS 12/11 (left panels). The depth-scale is the corrected composite depth (see text for details). Light gray symbols represent the data, whereas solid lines (blue and red) are three-point moving average curves. Light gray vertical dashed rectangles indicate the glacial maximum and interglacial periods, based on $\delta^{18}O$ record

3.2. B/Ca results

The B/Ca ratios obtained on the epibenthic species *C. wuellerstorfi* across transitions MIS16/15 and MIS12/11 are shown on figure 76. Following Yu and Elderfield (2007) and Yu et al. (2010), B/Ca of *C. wuellestorfi* is proportional to the ΔCO_3^{2-} (and thus the $[CO_3^{2-}]$) of bottom water.

Across transition MIS16/15, the B/Ca record suggests that bottom water $[CO_3^{2-}]$ was higher during the glacial than the interglacial. Two clear peaks are observed at 1895 cm and the second is centered at~1865cm, after which B/Ca drops to a minimum of ~150µmol/mol, before increasing slightly during the interglacial. Across transition 12/11, B/Ca shows also higher values during the glacial than the interglacial and two B/Ca peaks (~165 µmol/mol) at ~1335 cm and 1370 cm, and a major B/Ca decrease between 1300 cm and 1330 cm.

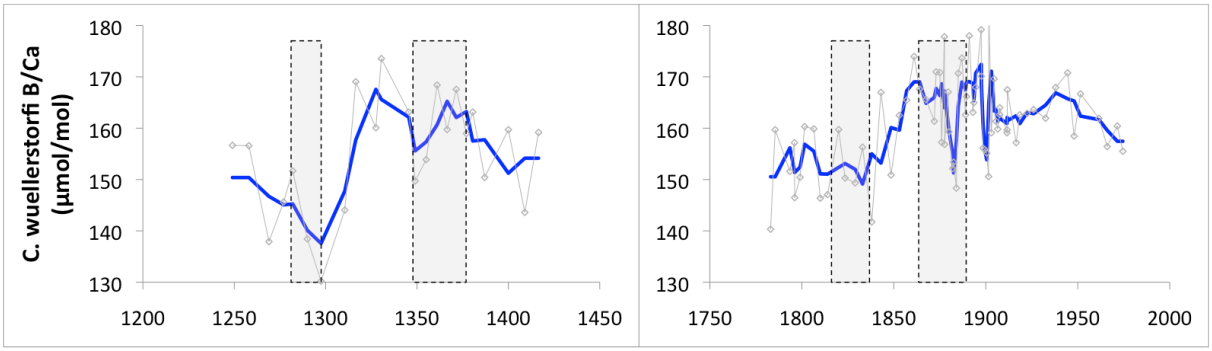

Figure 76 : B/Ca (µmol/mol) of the species *C. wuellerstorfi*, in µmol/mol, over the two transitions MIS 16/15 (right hand side, 70 data points) and MIS 12/11 (left hand-side, 23 data points). Light gray symbols and lines represent the measured data, whereas the blue solid lines represent the three-point moving average curves. Light gray Vertical dashed rectangles indicate the $\delta^{18}O$ stratigraphic control of the maximum glacial and interglacial periods (See figure 75 for explanation).

3.3. Results for the qualitative preservation/dissolution proxies

The changes in foraminifer fragmentation, %150µm, $\%CaCO_3$ and size-normalized weight of *N. dutertrei* are reported on figure 77. Foraminifer fragmentation has often been considered as a rather good proxy of carbonate preservation/dissolution (Thunell, 1976). At ODP Site 849, as can be readily seen from figure 77, the foraminifer fragmentation record clearly shares the strongest, common features with the %150µm record (obtained at higher resolution), confirming that grain size of deep-sea pelagic carbonate sediments seems to be chiefly controlled by preservation/dissolution of foraminifer shells at that location (i.e. Bassinot, 1993; Bassinot et al., 1994).

Across the transition MIS 16/15, the high-resolution %150µm record makes it possible to observe two peaks (high coarse fraction content) at 1895cm, 1880cm and a plateau at 1835cm within the deglacial decrease of the high coarse fraction. Although these features are not fully resolved in the other proxies (obtained at lower resolution), they correspond to levels of low foraminifer fragmentation and heavy *N. dutertrei* weight, all indicating a good preservation of carbonates.

Across the MIS 12/11 transition, the foraminifer fragmentation and the percentage of coarse fraction display, again, very similar patterns. As can be seen from Figure 77, low fragmentation and high %150µm (i.e. good preservation) are globally found in the glacial interval, whereas higher fragmentation/lower %150µm (i.e. stronger dissolution) are observed in the interglacial. Two clear preservation peaks are seen at 1370 cm and~1310 cm, with the second peak occuring during the deglaciation (see also $\delta^{18}O$ record in figure 75). The size-normalized mass of *N. dutertrei* also shows these two peaks to some extend, although the first one is not as marked as in the two above proxies. Although the carbonate content does share some common features (i.e. peak around 1370 cm), its variations seem to be slightly out of phase compared to changes observed in the other proxies (i.e. second peak around 1285 cm instead of 1310 cm).

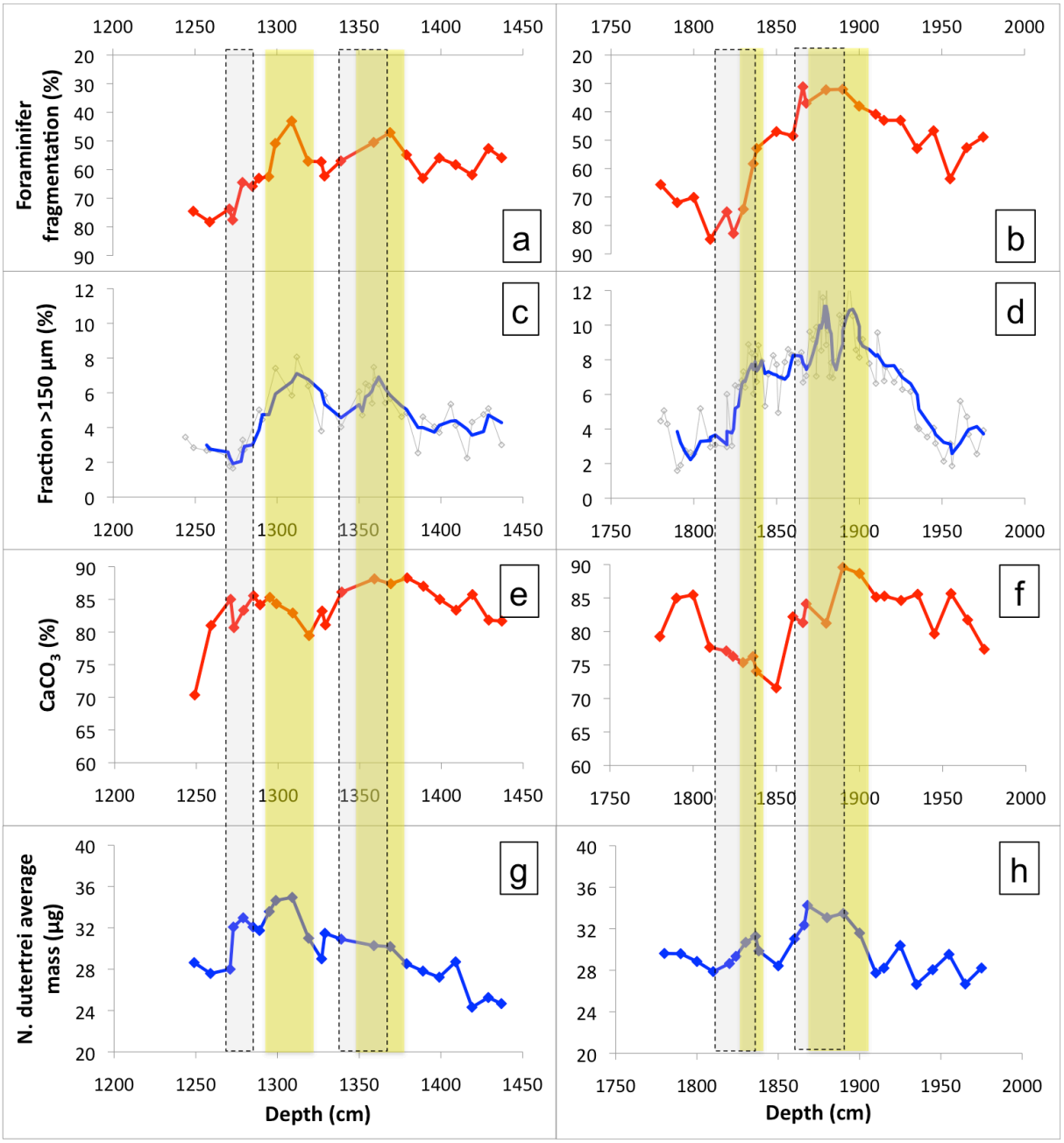

Figure 77 : Left panel: transition MIS 12/11; right panel: transition MIS 16/15. (a and b) percentage of foraminifers fragmentation (reversed scale); (c and d) percentage of the fraction >150 µm (light gray data, solid line 3 points moving average); (e and f) percentage of $CaCO_3$; (g and h) average mass of N. *dutertrei* (µg) in the 355-400 size fraction. Vertical dashed rectangles represent the $\delta^{18}O$ stratigraphic control of the maximum glacial and interglacial periods. Light yellow bars highlight the positions of the preservation peaks and the smaller plateau in the records.

Comparing the two glacial-interglacial transitions, the foraminifer fragmentation, the coarse fraction and the % carbonate indicate a higher preservation level during stage 16 than stage 12. A larger decrease of preservation occurs during the deglaciation following stage 16 to reach a similar level of preservation for

the two interglacial stages 15 and 11, as indicated by both the foraminifer fragmentation and the % of coarse fraction.

As can be seen from Figure 77, although the four sedimentological proxies do share some common features that likely correspond to carbonate preservation/dissolution changes, there also exist clear differences between the four records. Such differences confirm that those proxies, although affected by carbonate preservation/dissolution, are also affected by other factors such as surface productivity, dilution by non-carbonated material, winnowing, or changes in initial shell weight. In order to extract the common variability, which could be more confidently assigned to preservation/dissolution, we followed the approach proposed by Peterson and Prell (1985) and used Principal Component Analysis (PCA). As shown by Peterson and Prell from a careful multi-proxy study of preservation/dissolution along a depth transect in the Indian Ocean, the first component of such PCA analysis successfully extracts and amplifies the true preservation/dissolution signal. We performed the PCA analysis using the Analyseries software (Paillard et al., 1996). We used the inverse of fragmentation (i.e. preservation signal) so that the four records co-vary. The first principal component accounts for 52.4 % of the total variance shared by the four proxies. $CaCO_3$ accounts for the minor influencing parameter of this component (coefficient of 0.33), whereas inverse of fragmentation represents its major parameter (0.67).

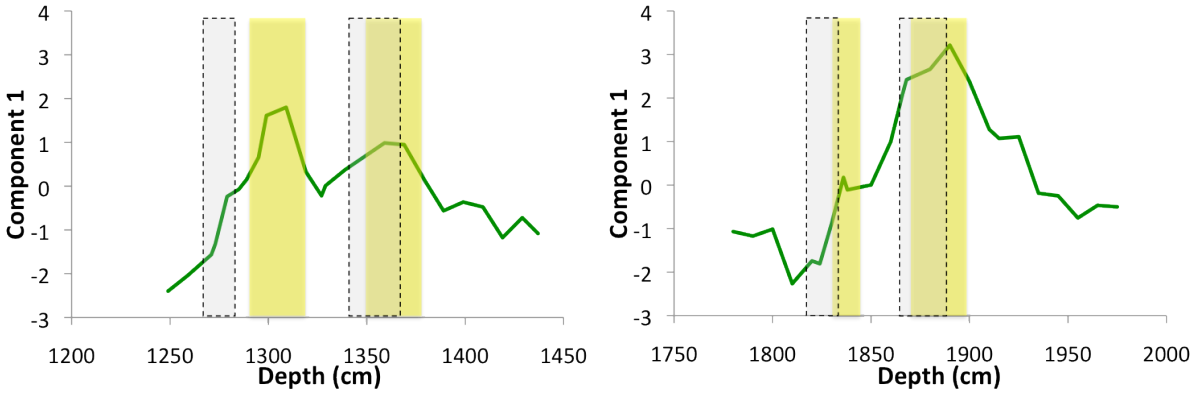

Figure 78 : Principal component analysis of the four qualitative proxies used in this study for the transitions MIS 16/15 (right panel) and MIS 12/11 (left panel). Y-axis is arbitrary but makes it possible to compare the two transitions, with high values corresponding to high preservation levels. Vertical dashed rectangles represent the $\delta^{18}O$ stratigraphic control of the maximum glacial and interglacial periods. Light yellow bars indicate the positions of the preservation peaks, as well as the small plateau recorded for MIS16/15.

The evolution of the first principal component is displayed on Figure 78. As can be seen from this figure, across transition 16/15, the PC1 values increase from about ~ 1950cm to reach maximum values at the glacial maximum (~1890-1870cm; with the highest PC1 value obtained at ~ 1880cm). PC1 starts to decrease before the end of the glacial maximum, and continues to decrease until the entire deglaciation, reaching a minimum value (~ 1810cm) at the end of the interglacial period. During the deglaciation, a small "shoulder" is observed in the PC1 record.

Regarding the MIS12/11 transition, the PC1 values increase from the bottom of the analyzed interval, reaching a peak within the glacial maximum of MIS12 (around 1370cm). Then, contrary to what is observed for MIS16/15, the deglaciation does not correspond to a rather monotonous decrease in PC1, but is rather characterized by the occurrence of a strong preservation peak (max around 1300cm), with values higher than those obtained during the glacial maximum (at 1370cm).

4.Discussion

4.1. Comparison of sedimentological preservation records with benthic B/Ca across MIS 12/11 and MIS 16/15: what do these proxies actually record?

For many years paleoceanographers had lacked a geochemical proxy, that could give directly access to the carbonate saturation state of bottom waters. Thus, in order to infer past changes in carbonate geochemistry of bottom waters, they studied the preservation of pelagic carbonate particles found in deep-sea sediments (e.g. Peterson and Prell, 1984; Farrell and Prell, 1989; Bassinot et al., 1994; Le and Shackleton, 1992; Broecker and Clark, 1999, 2001, 2002). Here, for the first time, we can compare past changes in the B/Ca content of the epibenthic foraminifer *C wuellerstorfi*, a proxy for bottom water [CO_3^{2-}] (Yu et al., 2007; 2010), with variations in deep-sea carbonate preservation/dissolution derived from the combination of four well-known proxies (foraminifer fragmentation, %coarse fraction, %$CaCO_3$ and size-normalized shell weight of foraminifer shells), combined in the first component (PC1) of the Principal Component Analysis.

Comparison of PC1 and B/Ca ratio of *C wuellerstorfi* across MIS16/15 and MIS12/11 is shown in figure 79. Our study clearly underlines the differences between the two deglaciations: both the PC1 and B/Ca records show a better preservation level during glacial maximum of stage 16 than during glacial maximum of MIS 12. However, the B/Ca record of MIS 12/11 shows, after the preservation peaks, a dissolution event that has a larger amplitude than for transition 16/15, with a steep decrease of ~40µmol/mol against only ~20µmol/mol for MIS 16/15 while the PC1 indicate, on the opposite, a larger preservation decrease for transition 16/15 than for transition 12/11. However, the preservation differences recorded in core ODP 849 by the B/Ca of *C wuellestorfi* are consistent with previous studies on the deep tropical Pacific from Farrel and Prell (1989); Murray et al. (2000) and Lalicata and Lea (2011). Our study indicates, therefore, that at site ODP 849 the "classical", sedimentological preservation proxies provide a qualitative record of temporal preservation/dissolution changes, but not a quantitative record (since amplitude of proxy changes do not seem to accurately reflect the amplitude of bottom water chemistry changes).

Another striking dissimilarity between the two transitions appears when we report on the same figure B/Ca and the PC1 (Figure 79). Across transition 16/15, B/Ca and PC1 seem to evolve in phase, whereas across transition 12/11, B/Ca varies before the other proxies. A cross-correlation of the two proxies during each time periods gives a correlation of 0.65 with no lag for transition 16/15, but a ~28cm offset of the B/Ca signal is necessary to obtain the best correlation (0.78) for transition 12/11.

Figure 79 : Comparison of the evolution of *C. wuellerstorfi* B/Ca (blue, left-hand scale) and First Principal Component calculated from the PCA of sedimentological, carbonate preservation proxies (green, right-hand arbitrary scale). Vertical dashed rectangles represent the $\delta^{18}O$ stratigraphic control of the maximum glacial and interglacial periods.

If preservation of carbonate material on the sea floor and saturation state of bottom water were closely related, we should have found a direct, in-phase relationship between B/Ca and PC1. It is the case for transition 16/15, but it is not true for transition 12/11 (it should be noted that none of the initial sedimentological proxies gives a better, more direct correlation to B/Ca).

It is particularly the deglacial preservation signal at the MIS 12-11 transition that shows the stronger, out-of-phase behaviour between benthic foraminifera B/Ca and the PC1. What kind of processes could drive the response of qualitative, sedimentological preservation proxies in such a way that these proxies show a temporal evolution that appears to be out-of-phase with respect to the bottom water carbonate ion concentration? We believe that the evolution of the carbonate productivity along the deglaciation could explain this behaviour. A decrease of the carbonate productivity in the first part of the deglaciation would produce a decrease in the percent carbonate even if the carbonates are well preserved at the seafloor. Such a drop in carbonate productivity would also drive a decrease in the % coarse fraction resulting from the relative increase of dilution by fine, non-carbonate material. The foraminifer fragmentation is more puzzling. In order to fit with our hypothesis, the increase in foraminifer fragmentation would have to be the result of a changing assemblage: the lower productivity being linked to a more oligotrophic assemblage with, for example, more *G. ruber* specimens, that are more fragile and subject to dissolution. On the second part of the deglaciation (1325 to 1250 cm) an increase in the productivity would again produce an opposite effect on the sedimentological carbonate preservation proxies counteracting the effects of the large decrease in bottom water carbonate concentration that is indicated by the B/Ca concentration of benthic foraminifera. The initial shell weight of *N. dutertrei* could be increased during

such high productivity period as the result of fast growth rates, or the increase of sea surface CO_3^{2-} in relation to increased primary productivity and the efficient pumping of CO_2 by photosynthetic activity.

To evaluate the time lag between the proxies and to compare our data to atmospheric carbon evolution, we developed an age model for core ODP849 for the two glacial-interglacial transitions. This will allow to compare our records to Yu et al. (2010) records to investigate whether such a phase lag exists in different areas and/or different time periods.

4.2. Age model for core ODP 849

As we changed the jonction of the different ODP cores, we could not keep the previous age scale of Mix et al. (1995). We thus tuned our benthic $\delta^{18}O$ record to Lisiecki and Raymo (2005) benthic stack using Analyseries software.

4.3. Comparison of ODP 849 terminations V and VII records with the record of the last deglaciation

To date, only few studies have used the B/Ca as a proxy of deep-water carbonate ion saturation. Most of these studies focused on the last deglaciation or the last glacial cycle (Yu et al., 2010; Raitsch et al., 2011), or offered an overview of last 800ka (Rickaby et al., 2010) or older periods like Cenozoic (Brown et al., 2011), but with a lower resolution. Yu et al. (2010) compared the B/Ca record of cores from different oceanic basins through the last deglaciation. First of all, they also noted that other sedimentological preservation proxies could mirror or not the B/Ca record of *C. wuellerstorfi* depending on the cores. It is clear that local factors, such as the increased productivity we observed for MIS 12/11 transition in core ODP849, will interfere with the bottom water bicarbonate concentration to control the final preservation/dissolution of carbonate material and, thus, the variations of sedimentological preservation proxies.

Comparing the B/Ca records from cores obtained in different basins, Yu et al. (2010) highlighted the role of circulation changes on deep-water carbonate concentration changes. They indicated that the B/Ca record of a core, retrieved in the Pacific Ocean, at a shallower depth than ODP849, underwent probably the influence of the changing depth of North Pacific deep water between glacial and interglacial periods. Thus, in order to compare the evolution of deep water carbonate concentration at the three different terminations, we choose to compare our Pacific record with the Indian Ocean core WIND 28K studied by Yu et al (2010). This core, retrieved at 4147 m depth, is bathed by Southern deep waters like our ODP site 849. The core is representative of the wide Indo-Pacific deep waters and the percent carbonate content record of this core mirrors its B/Ca record, indicating no local influence that would complicate the dissolution signal.

In figure 80, our data sets (terminations V and VII) are compared to those obtained by Yu et al. (2010) on core WIND28K on the last deglaciation. To consider the different mechanisms that have modified the deep water carbonate concentrations, we compared the *C. wuellerstorfi* B/Ca signal to other climatic signals from the same cores. From bottom to top, for each termination are also presented the isotopic oxygen and

carbon composition of the same benthic foraminifera species (*C. wuellerstorfi)*, the carbon isotopic composition of the planktonic *N. dutertrei* foraminifera and the carbon atmospheric evolution.

During the last deglaciation, core WIND 28K presents an increase in B/Ca that begins synchronously with the $\delta^{18}O$ increase at about 17 kyr. The B/Ca stops to increase around 14ka Cal BP, and remains relatively stable for about 4 kyr, until ~ 10 Cal kyr BP. This defines a "deglacial B/Ca peak". Then the B/Ca decreases during the Holocene until ~5 kyr, with a B/Ca level higher in glacial than in interglacial. Yu et al. interpreted the first B/Ca increase as the deep water carbonate concentration increase resulting from the rapid CO_2 degassing through Southern Ocean upwelling at the early beginning of the termination.

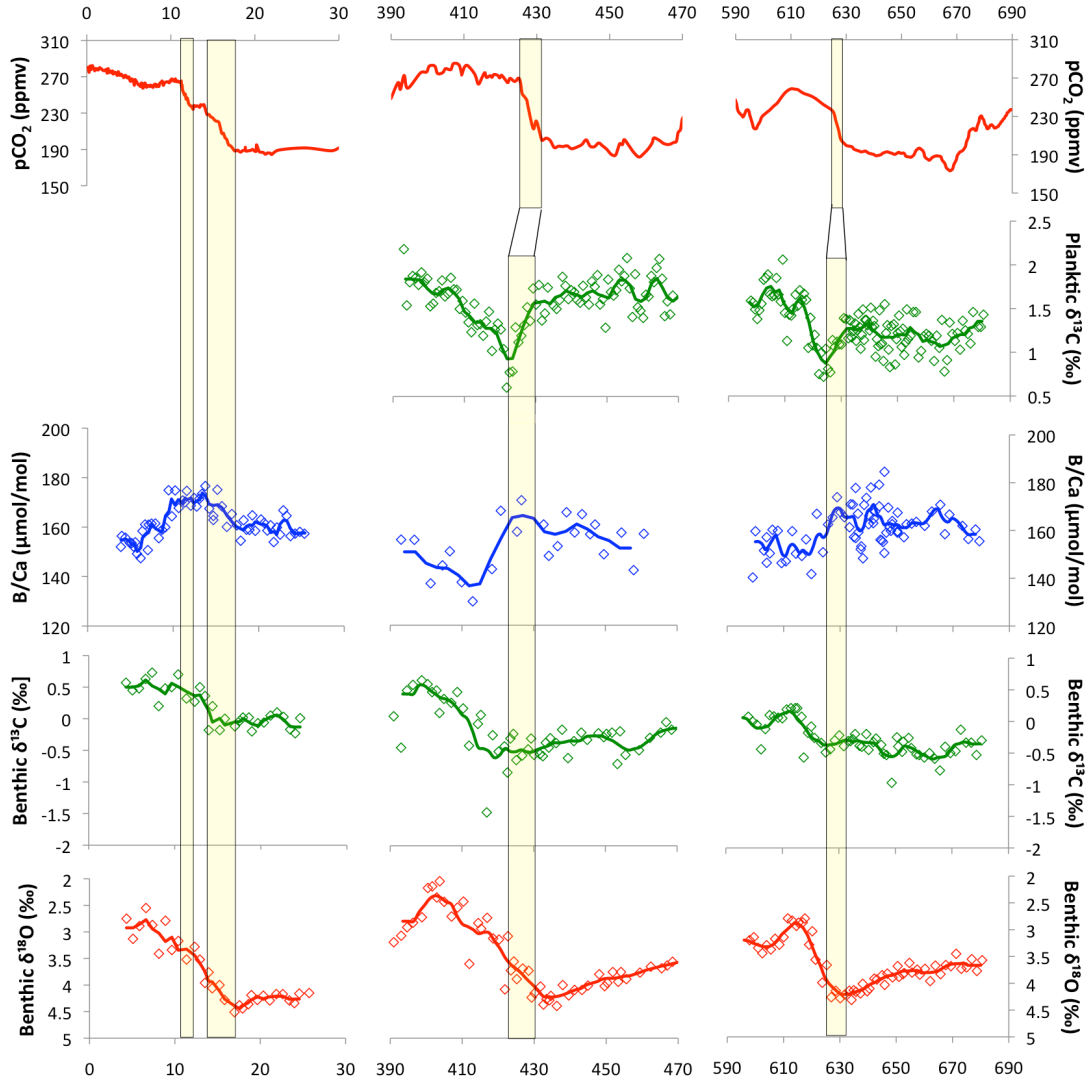

Figure 80 : Evolution of (from bottom to top): benthic $\delta^{18}O$ (‰), benthic $\delta^{13}C$ (‰), B/Ca (µmol/mol), planktic $\delta^{13}C$ (‰) and atmospheric pCO_2 (ppmv) across the terminations I (Yu et al., 2010), V and VII (this study) . Vertical rectangles indicate the correlations made between sharp increases of pCO_2 and rapid decreases of planktic $\delta^{13}C$ to link the other proxies to the atmospheric record for transition V and VII. For transition I, the records are presented with their own age scale and vertical rectangles highlight the rapid atmospheric CO_2 increase.

The stable B/Ca plateau that follows is the result of a balance between

i) continuous CO_2 outgassing of the Ocean to the atmosphere and the terrestrial biosphere starting to grow (as indicated by the increase in benthic $\delta^{13}C$) and

ii) the carbonate compensation effect that started after the preceeding B/Ca increase. Indeed, the carbonate compensation effect starts to be significant after 2 000 to 5 000 yr (Archer et al., 1991; Broecker and Peng, 1987)

The third phase of the B/Ca WIND 28K record is a decrease through the Holocene toward a lower bottom water CO_3^{2-} value than the glacial one.

The two transitions that we studied in ODP Site 849 show some similarities, and striking differences compared to the deep Indian and Pacific records of the last termination studied by Yu et al. (2010).

As far as similarities are concerned, the evolution of benthic $\delta^{13}C$ relative to $\delta^{18}O$ changes is similar in all cases, with relatively stable values of benthic $\delta^{13}C$ during the first part of each one of the two deglaciations, followed by a sharp increase in $\delta^{13}C$ that occurs during the second part of all the deglaciations. However the time lag between $\delta^{18}O$ and $\delta^{13}C$ changes is more than twice as long for termination V than for termination VII. In terms of B/Ca changes, as is observed for the Indian record WIND28K, the two old G/IG transitions in the Pacific show higher B/Ca during early glacials than during interglacials.

As far as differences are concerned, it is readily obvious that the Indian core shows an increase in B/Ca in the first part of the deglaciation, with a peak occurring at about mid-deglaciation, whereas the two ODP 849 G/IG transitions show early increases in B/Ca, starting in the glacials, with peak values reached before the glacial maxima. Across MIS16/15, there is no apparent B/Ca peak during the deglaciation, while across MIS12/11 transition, there is an early peak, occurring in the first third of the $\delta^{18}O$ decrease.

These results raise many interrogations about whether similar mechanisms have driven these three deglaciations. Let us summarize some important pieces of information:

1/ the B/Ca record shows higher B/Ca in glacials than interglacials, so if B/Ca truly reflects bottom water ΔCO_3^{2-} and hence $[CO_3^{2-}]$, this result suggests a better preservation of deep Pacific carbonates in glacials than interglacials at ODP Sit 849, which is consistent with the results obtained by several authors (Farrell and Prell, 1989; Archer, 1991; Hodell et al., 2001, 2003)

2/ the benthic foraminifera $\delta^{13}C$ records display a similar evolution in regard to the $\delta^{18}O$ ones for the three deglaciations, which suggests the strong influence of terrestrial biosphere oceanic carbon budget in the later part of the deglaciations (Kaplan et al., 2002; Broecker et al., 1999; Yu et al., 2010; Brovkin et al., 2012)

3/ at the Indian Ocean site (4000m), the Termination I is characterized by an increase in B/Ca in the first part of the deglaciation, followed by a plateau more or less synchronous with the benthic foraminifera

$\delta^{13}C$ increase. In the ODP site 849, however, both terminations V and VII show a B/Ca increase during the glacials, with peak values reached before the beginning of deglaciations, much earlier than the $\delta^{13}C$ benthic foraminifera increase. In the MIS12/11 transition, a second peak is taking place during the early deglaciation, still out-of-phase with the $\delta^{13}C$ increase.

In order to better understand the scenario of these deglaciations, one needs to analyze the timing of the B/Ca preservation peaks compared to the CO_2 outgassing from the ocean. Is this rapid deglacial outgassing occurring through the upwelling of the Southern Ocean and when does it occur compared to the large Ice Sheet melting represented by Pacific deep ocean benthic foraminifera $\delta^{18}O$ decrease?

We cannot rely on the direct comparison of the ice core atmospheric CO_2 record and the ODP isotopic and B/Ca records as the age scale error might be larger than the outgassing period we are looking at. However the ODP 849 core being located on the border of the Pacific equatorial upwelling, the period of rapid deep ocean CO_2 outgassing through the Southern Ocean upwelling is marked by rapid, large amplitude decrease in planktonic $\delta^{13}C$ (Spero et al., 2002; Toggweiler, 1999; Toggweiler et al., 2006). At both Termination VII and V, such a rapid decrease occurs in the *N. dutertrei* carbon isotopic record, with a larger amplitude at termination VII than at termination V. Thus, assuming that the rapid increases of atmospheric CO_2 at the termination VII and V are coeval with the decrease of planktonic $\delta^{13}C$ in core ODP849, we observe that this rapid CO_2 oceanic outgassing is associated with the preservation peak indicated by the B/Ca record. These outgassing periods occur on the very beginning of the deglaciation as indicated by benthic oxygen isotopic signal but last longer at the MIS 12-11 deglaciation.

At both terminations VII and V (ODP Site 849) B/Ca drops after these short preservation events while at the last termination (core WIND 28K) the increase and plateau of B/Ca last for all the termination and the B/Ca starts to drop only during the Holocene. Though the benthic $\delta^{13}C$ increases in the following part of the deglaciation, indicating the regrowth of the terrestrial biosphere (Kaplan et al., 2002; Broecker et al., 1999; Köhler et al., 2005; Yu et al., 2010; Brovkin et al., 2012). However the rate at which the Ocean is outgassing CO_2 to the atmosphere and biosphere can still be inferred from the Ice core atmospheric CO_2 record. In the following table 13, the atmospheric CO_2 increase and the time interval for the different increasing periods of the 3 terminations are indicated.

Termination	**I**	**I**	**V**	**VII**
Time period (ka)	10.8 - 12.6	14 - 18	425 - 435	625.5 - 629.5
pCO_2 increase (ppmv)	25.4	50.0	70.0	35.5
pCO_2 increase rate (ppmv/kyr)	15.9	12.5	7.0	8.9

Table 13 : Periods of the terminations I, V and VII, encountering the major increases of pCO_2 of these deglaciations, together with their range of variation and increase rate of pCO_2.

While at termination VII and V there is only one period of rapid and huge increase of atmospheric CO_2, the last deglaciation is marked by two very rapid increase in the atmospheric CO_2. The second rapid increase is coeval to the B/Ca plateau in core WIND 28K, which suggests that the preservation event that should result from CO_2 outgassing is counterbalanced by the delayed deep carbonate compensation associated to the first atmospheric CO_2 increase through Southern Ocean outgassing. After this second rapid increase the CO_2 slowly increases from 260 to 280 ppmv over the next 8 kyr. Thus, the deep carbonate compensation following the two Southern Ocean outgassings dominates and the B/Ca decreases along the Holocene.

For the older Terminations (ODP 849), only one rapid outgassing period it shown by ice core record after which the rate of atmospheric CO_2 outgassing rapidly decreases. Thus, the carbonate compensation resulting from this first rapid outgassing is not balanced by the increase in deep water preservation associated to the slow CO_2 outgassing occurring during the second par of the termination.

For termination V the B/Ca decrease is even larger, which is probably due to a worldwide increase in carbonate productivity, which induces a decrease of bottom water preservation through the carbonate compensation mechanism (Barker et al., 2006). This productivity increase that we observe at the ODP 849 location (see 4.1) delays the increase in the benthic foraminifera $\delta^{13}C$ and produces an "overshoot" towards low B/Ca values, due to increased carbonate compensation mechanism in response of the larger carbonate flux to the sea floor, before the stabilization at a similar B/Ca value for stage 11 than for stage 15.

4.4. Quantification of CO_3^{2-} at terminations VII and V, comparison with the last deglaciation: conversion of the B/Ca signal to bottom water ΔCO_3^{2-} and $[CO_3^{2-}]$

Yu and Elderfield (2007) have shown that there exists a direct, linear relationship between carbonate ion saturation (ΔCO_3^{2-}) and the B/Ca of several benthic foraminiferal species, including *C. wuellerstorfi* (eq. 1). This species has two advantages: (1) its B/Ca shows a strong linear relationship to bottom water ΔCO_3^{2-}, with a steep slope, and (2) it is an epibenthic foraminifer, which insures that the B/Ca reflects bottom water chemical signature and not some pore water signature that could be affected by early diagenesis (i.e. oxidation of organic carbon, dissolution of calcite,..).

The empirical calibration of *C. wuellerstorfi* B/Ca with respect to bottom water $\Delta CO_3^{2-}$was established using core tops from the Norwegian Sea and Atlantic, Indian and Pacific oceans (Yu et al., 2007). For this empirical calibration, Yu and co-authors have fitted a linear regression equation through their entire dataset. However, has can be readily seen from figure 81, the Indo-Pacific data points located in the undersaturated range of ΔCO_3^{2-} in the graph (from about 0 down to -20 µmol/kg) seem to be mostly situated under the regression line. It is possible that the small number of Pacific samples ($\sim$ 55) compared to the Atlantic and Norwegian sea samples ($\sim$100) result in a poor constrain of the regression line in the

low ΔCO_3^{2-} area. But we cannot reject the possibility that the Atlantic/Norwegian samples, in the one hand, and the Pacific samples, on the other hand, do align along two distinct regression lines. A first possible explanation for the existence of two distinct datasets at high and low ΔCO_3^{2-}, respectively, could be the partial, *post-mortem* dissolution of benthic foraminifer shells bathed by undersaturated bottom waters. As we have shown for planktonic foraminifers (Coadic et al., in revision, chapter III of this manuscript), the partial dissolution of foraminifer calcite results in the preferential loss of B relative to Ca. This could explain why the deep-Pacific samples show anomalously low B/Ca in figure 81. Another potential explanation could be an ontogenic effect linked to foraminiferal growth under undersatured conditions. However, none of these possibilities can be tested with the data in hands. This aspect requires further studies, ideally based on cultured benthic foraminifers in order to better constrain the effect of (very) low saturation on the B/Ca proxy, avoiding the potential bias of micro-environment specific to each sample site.

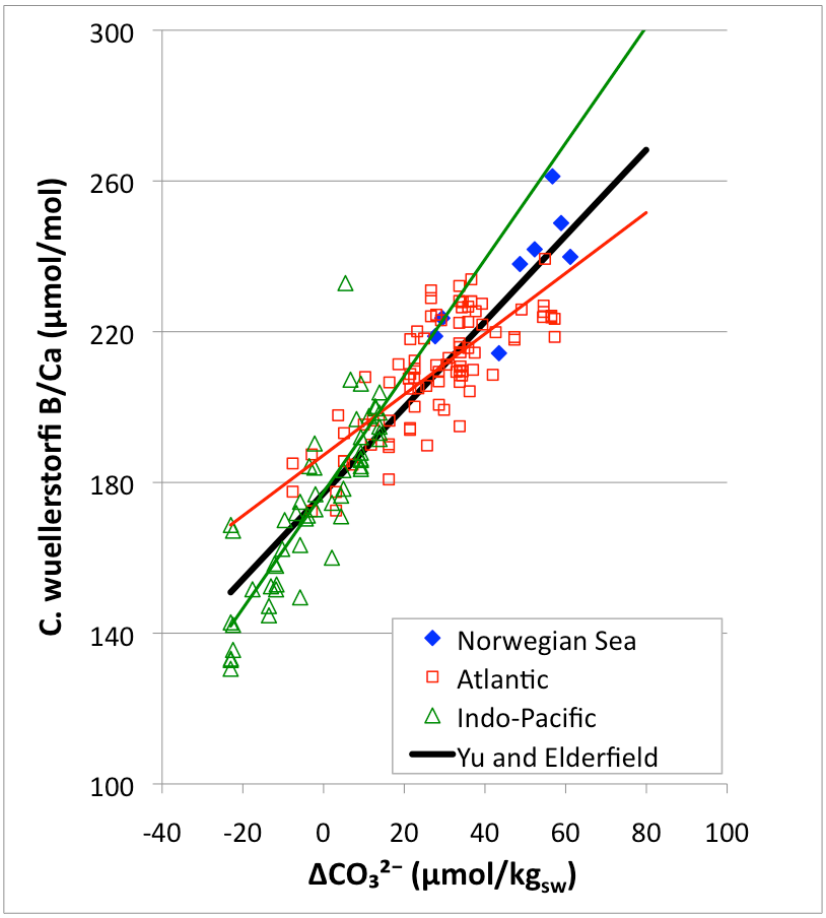

Figure 81 : B/Ca of *C. wuellerstorfi* as a function of seawater ΔCO_3^{2-}. The black line represents the regression equation obtained by Yu and Elderfield (2007): B/Ca = 1.14 ΔCO_3^{2-} + 177.1 (R^2=0.86). The green and red lines are linear regressions obtained using the Indo-Pacific and Atlantic samples, respectively. The linear regression equation for the Indo-Pacific: B/Ca = 1.54 (±0.13) ΔCO_3^{2-} + 177.4 (±2) (R^2=0.73, n=55); and for the Atlantic: B/Ca = 0.80 (±0.07) ΔCO_3^{2-} + 187.2 ± (3) (R^2=0.61, n=91).

In this paper, in order to estimate the impact of calibration on the final estimation of bottom water [$CO_3^{=}$] during the MIS 12/11 and MIS 16/15 transitions, we used both (i) Yu and Elderfield (2007)'s global calibration and (ii) the more specific calibration curve obtained by keeping only the Indo-Pacific samples (figure 81). The two calibrations show significantly different slope coefficients.

The carbonate ion saturation represents the difference between in-situ [CO_3^{2-}] and the CO_3^{2-} at saturation ([$CO_3^{2-}]_{sat}$) for the given carbonate species (i.e. calcite, aragonite...). Using past sea-levels and deep-Pacific temperatures reconstructed by Sidall et al. (2010), and subsequent estimates of salinity, alkalinity and dissolved inorganic carbon (DIC), we computed that, at the water depth of our site ODP 849, the $[CO_3^{2-}]_{sat}$ had a mean value of 90.7±0.6 (2σ) µmol/kg at the glacial maxima of the two transitions MIS 12/11 and MIS 16/15. This value falls very close to the preindustrial saturation CO_3^{2-} value of 90.2 µmol/kg obtained with the GLODAP data set (Key et al., 2007). Moreover, the range of variations between a glacial and an interglacial stage remains small, due to the small offsetting effects of several parameters such as temperature and pressure (sea-level). Hence, we used a constant $[CO_3^{2-}]_{sat}$ together with our boron-based ΔCO_3^{2-} estimates to calculate past changes in [CO_3^{2-}] across the two G/IG transitions.

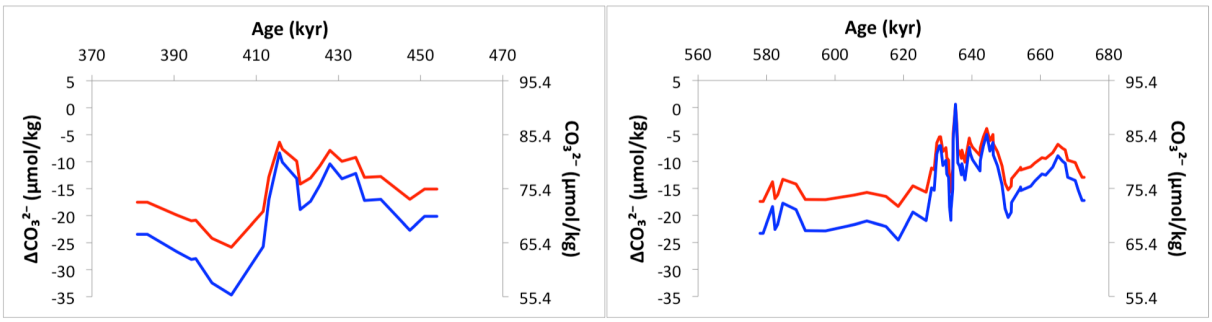

Figure 82 : Variations of bottom water carbonate ion concentrations across MIS12/11 (left panel) and MIS16/15 (right panel). For each graph, two scales are given: [ΔCO_3^{2-}] (left Y-axis) and [CO_3^{2-}] (right Y-axis). In red are displayed the results obtained using our Indo-Pacific calibration, and in blue are displayed the results obtained with Yu and Elderfield (2007)'s original calibration.

As can be readily seen from figure 82, the use of one or the other calibration equation not only change the absolute values, but has also a small impact on the amplitude of carbonate changes during the deglaciation (Figure 82, Table 14). Furthermore, we should emphasize that these absolute values might be modified when an international calibration for B/Ca foraminifera will take place. During MIS 12, carbonate ion increases by 10 to 11 µmol/kg and reaches its two maxima, before dropping by 19 to 24 µmol/kg during the deglaciation. MIS 16 show a similar evolution, with a [CO_3^{2-}] increase of 9 to 13 µmol/kg, but a smaller drop during deglaciation of 10 to 14 µmol/kg.

	Transition MIS 12/11		Transition MIS 16/15	
	Yu and Elderfield	Indo-Pacific	Yu and Elderfield	Indo-Pacific
Glacial mimimum	68	73	71	76
Peak 1	80	83	84 (91*)	85 (91*)
Low between peaks	72	72	76	77
Peak 2	80	83	83	85
Interglacial minimum	56	64	69	75

Table 14 : Carbonate ion maxima and minima estimated during the transitions MIS 12/11 and MIS 16/15, and reconstructed either with our Indo-Pacific calibration or Yu and Elderfield (2007) original calibrations. (*) marks the highest values recorded for $[CO_3^{2-}]$, at the end of the first preservation peak.

The estimated increase in $[CO_3^{2-}]$ to reach the preservation maxima is consistent with the amplitude of variations recorded by Yu et al. (2010) on both cores WIND 28K and MW91 GGC48, which showed a 10-11µmol/kg change between a CO_3^{2-} minimum at the LGM and the maximum reached during the second part of the deglaciation. Transition MIS16/15 presents a similar amplitude (from 10 to 14), whereas transition 12/11 shows an even stronger drop in CO_3^{2-} that has been discussed previously. Furthermore both MIS 12 and MIS 11 values are lower than MIS 16 and MIS 15 values. This is in agreement with the 400 kyr dissolution cycle shown by Peterson and Prell (1985) and Bassinot et al. (1994).

Conclusions

Our deep tropical Pacific Ocean records underline the differences existing between transitions MIS 12/11 and MIS 16/15 and the last deglaciation. Results show a better preservation during glacial than interglacial, and a better preservation during MIS 16/15 than during MIS 12/11, but also display at preservation peaks occurring at the very beginning of the deglaciation as indicated by the benthic foraminifera isotopic decrease. Transition 12/11 points out a phase lag between preservation maxima of quantitative B/Ca records and qualitative sediment-based records, which may be explained by an increase in biogenic carbonate production, whereas transition 16/15 do not show this phase lag. Comparison of our data with last deglaciation records show rather similar variations across the three deglaciations, and similar amplitudes of $[CO_3^{2-}]$ changes. Our data suggest that similar mechanisms have driven deep ocean chemistry changes across the first part of these G/IG transitions: a preservation increase resulting from Southern Ocean CO_2 outgassing. The second part of the Termination differs from the two older deglaciations indicating a decrease in deep water carbonate concentration due to carbonate compensation increase, while for the last Termination, this carbonate compensation is balanced by a second Southern Ocean CO_2 outgassing event, and the deep sea carbonate concentration indicates a plateau for the final part of the deglaciation (defined as the period of benthic isotopic composition decrease).